ACS OMEGA

http://pubs.acs.org/journal/acsodf

Article

Preparation of ZnO-Incorporated Porous Carbon Nanofibers and Adsorption Performance Investigation on Methylene Blue

Du Nie, Ping Wang, Chuanfeng Zang, Guangyu Zhang, Suying Li, Rong Liu, Yu Zhang, Guang Li, Yi Luo,* Wei Zhang,* and Jiamu Dai*

Cite This: *ACS Omega* 2022, 7, 2198−2204

Read Online

ACCESS | Metrics & More | Article Recommendations | Supporting Information

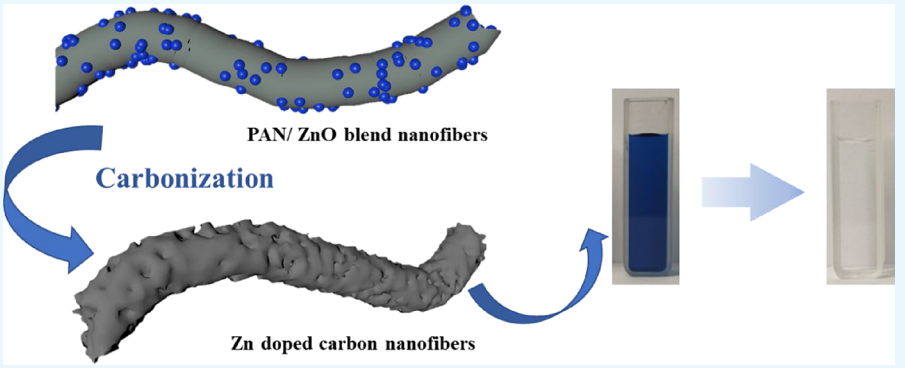

ABSTRACT: To improve the adsorption performance of carbon materials, novel ZnO nanoparticle-incorporated porous carbon nanofibers (Zn@PCNFs) were prepared via an electrospinning technique. A facile one-step fabrication strategy was proposed to simultaneously complete the carbonization of a peroxided polyacrylonitrile framework, the activating treatment caused by ZnO reducing to Zn, and the pore generation caused by evaporation of reduced Zn with a low melting point. The influences of the pH, ion category, and concentration on methylene blue adsorption were investigated. The physical−chemical characterizations showed that ZnO was homogeneously distributed on the nanofibers and micropores were generated. The adsorption results revealed that an efficient adsorption was obtained within a large range of pH values through different adsorption models, which was accelerated by increasing the temperature. Therefore, the novel Zn@PCNFs are anticipated to be applied in the future as an effective dye waste adsorbent.

1. INTRODUCTION

Various dyes and additives are applied in the fields including textile, chemistry, and medical treatment, and the lead dye waste water with dramatically increased amount and category become one of the main water pollutants nowadays.[1,2] Additionally, the condition complexity of dye waste water always makes purification hard.[3−5] Therefore, as a kind of workable and efficient method, adsorbents are applied to separate pollutants from water resources.[6,7] Carbon materials with a high specific surface area are widely used adsorbing agents in water treatment to remove organic pollutants or heavy metal ions.[3,8,9]

The structure and raw material would affect the adsorption performance and characteristic. For instance, graphene oxide (GO) has a high specific surface area and rich oxygen-containing groups,[10,11] which lead to a high dye adsorption efficiency through a hydrogen bond,[12] $\pi-\pi$ stacking effect,[13] and covalent bond.[14] The carbon adsorbing agents prepared by direct carbonization from wood or coal showed a lower adsorption efficiency due to a limited specific surface area or polar groups, and surface modification of activating treatment was usually applied.[15−17] Biochar need no activating treatment, but their adsorption efficiency was also low and was influenced by their raw material composition and carbonization temperature.[18,19] Cellulose-based carbon adsorbents, usually with a microsphere shape, have a worse pore structure, which needs further morphology modification to improve hydrophilicity and adsorption capacity.[20]

As traditional adsorbents, active carbon fibers (aCFs) were widely used in adsorbing pollutants from air and liquid. The larger amount and more shallow pores of aCFs result in a faster adsorbing−desorbing speed.[19,21] Meanwhile, the strong activity of aCFs provides special convenience in adsorption

Received: October 13, 2021
Accepted: December 24, 2021
Published: January 4, 2022

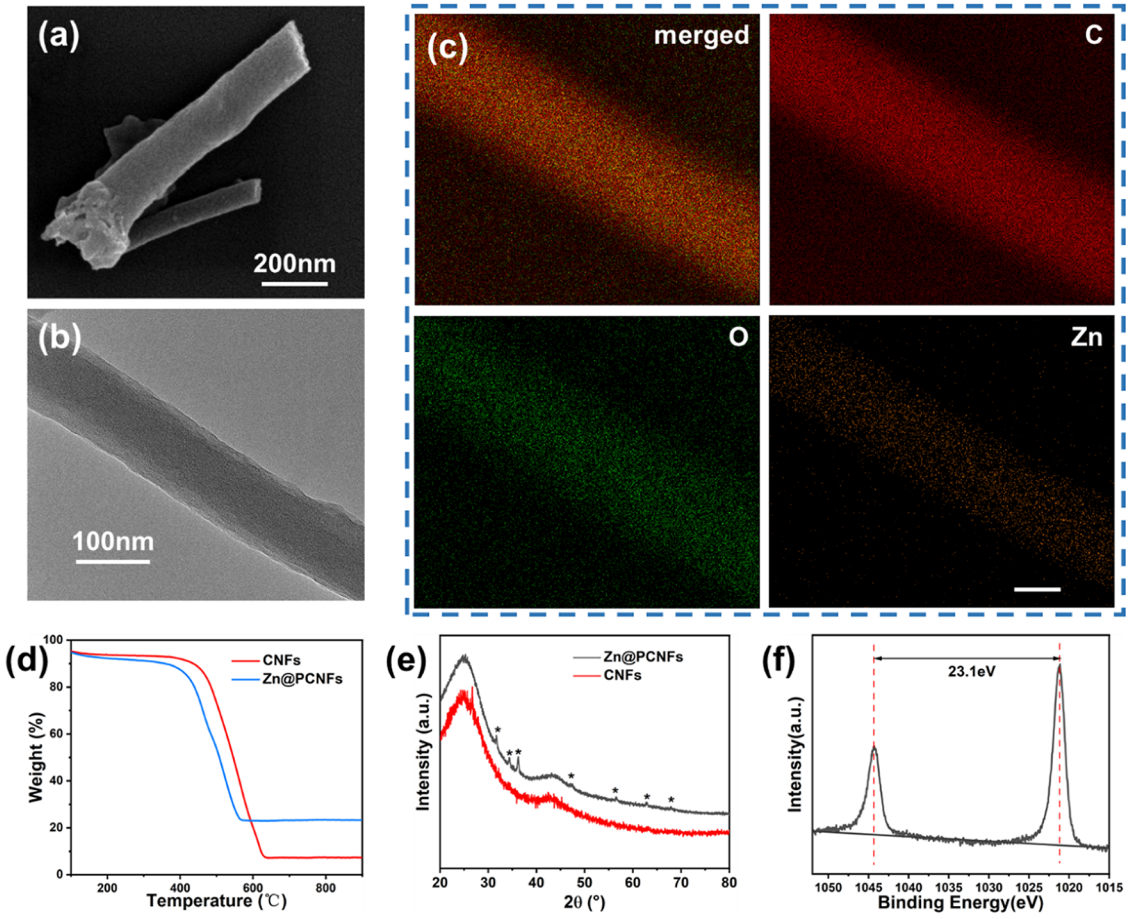

Figure 1. (a) SEM, (b) TEM, and (c) EDS mapping images (scale bar = 50 nm) of Zn@PCNFs. (d) TGA and (e) XRD analysis of nanofibers with or without Zn doping. (f) XPS survey spectra of Zn of Zn@PCNFs.

as well as further modification through a novel preparation method or incorporation with nanomaterials.[22−24]

To obtain the properties and porous structure of activated carbon for strong adsorption of ions or organic dyes, carbon materials usually need to undergo an activating treatment under temperatures higher than 600 °C and be exposed to an oxidation medium like KOH, which sometimes need assistance of a special atmosphere.[2,16,23,25] As a result, a higher energy will be required at the stages including the carbonization process of carbon precursors and the activating treatment. In addition, after the activating treatment, carbon materials will be further washed and dried to obtain the activated samples.[25] However, the pore size distribution is not easy to control.

A simple electrospinning technique was applied to prepare carbon nanofibers (CNFs) as reported in our previous work.[26] However, reported studies about CNFs in the field of adsorption were rare. In this study, ZnO nanoparticles were introduced in CNFs to obtain Zn-incorporated porous carbon nanofibers (Zn@PCNFs) with a strong adsorption performance. Through incorporating ZnO, pores or defects would be generated and pore size distribution would also be regulated. The chemical composition and structure were characterized by various experiments. For adsorption capacity measurements, methylene blue (MB) was chosen as the adsorbing object, and the influences of the pH value, MB concentration, temperature, and ion category were investigated. Afterward, adsorption models were applied to analyze the mechanism of the adsorption behavior. We believe that this work will provide important information for preparing a novel adsorbent for dye waste water treatment.

2. RESULTS AND DISCUSSION

2.1. Characterization of Zn@PCNFs. The morphology of Zn@PCNFs is shown in Figure 1a,b; the SEM and TEM images present that a good nanofiber structure was well formed (Figure S1) with diameters about 100 nm after carbonization of PAN/ZnO blend nanofibers, while the diameter of CNFs was about 350 nm (Figure S2). The specific surface area was 447.707 m^2/g with a wider pore size distribution (Figure S3), indicating that pores were generated and the porosity was better than that in CNFs (159.647 m^2/g) through ZnO incorporation because the reduced Zn species, whose melting point is 419.5 °C, were melted at 800 °C and partially evaporated. The Zn element was homogeneously distributed on the nanofibers according to the EDS mapping images (Figure 1c). Additionally, based on TGA (Figure 1d), the weight loss values of CNFs and Zn@PCNFs were 92.71 and 76.72%, respectively, revealing that the Zn element partially remained in the nanofibers. The mass proportion of zinc in Zn@PCNFs was 0.7684%, as checked by ICP. During the process of carbonization, PAN was converted to a carbon framework and partial ZnO were reduced to Zn and further evaporated due to their low melting temperature.[22]

To determine the form of the remaining Zn elements, the crystal structure of Zn@PCNFs was analyzed based on an XRD test. As shown in Figure 1e, two strong peaks at 20 and

https://doi.org/10.1021/acsomega.1c05729
ACS Omega 2022, 7, 2198−2204

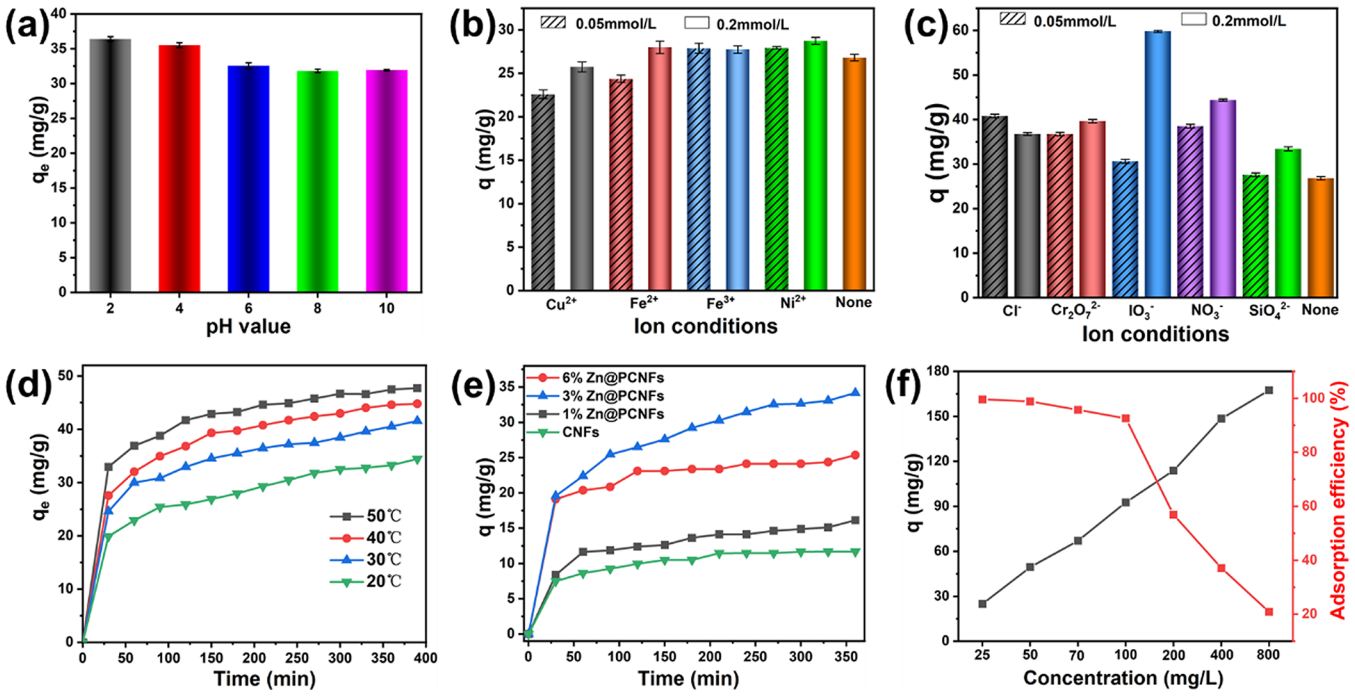

Figure 2. Effects of the (a) pH, (b) cation and (c) anion, (d) temperature, and (e) Zn content on the adsorption characteristics of MB from an aqueous solution using Zn@PCNFs. (f) Effects of the MB concentration on the adsorption capacity and decolorization rate of Zn@PCNFs.

44.4° appeared on the curve of CNFs, which were (002) and (100) of the typical graphite structure.[17,27,28] However, a series of sharp peaks at 31.8, 34.5, 36.2, 47.5, 56.5, 62.8, and 67.8° appeared on Zn@PCNFs, which were (100), (002), (101), (102), (110), (103), and (112) of ZnO, respectively.[29] Meanwhile, all ZnO peaks would disappear after acid wash of Zn@PCNFs (Figure S4). XPS was also performed to distinguish the form of the Zn element. The XPS spectrum of Zn is presented in Figure 1f; two peaks at 1022.0 and 1045.1 eV were found, which correspond to 2p3/2 and 2p1/2 of Zn, respectively, further revealing the existence of ZnO.[22]

2.2. Adsorption Test of Zn@PCNFs. Various aspects on MB adsorption were investigated. As shown in Figure 2a, the MB adsorption capacity of Zn@PCNFs was slightly increased (from 44.28 to 49.95 mg/g, 12.8%) with the increase in the pH value (from 2 to 10). MB could be ionized to a positive charge when dissolved in water,[30] and the point of zero charge (Figure S5) was evaluated as pH_{MB} (7.65) > pH_{pzc} (7.15), which would be attracted by negatively charged Zn@PCNFs (Figure S6). With decreasing of the pH value, Zn@PCNFs would be protonated and generate electrostatic repulsion to MB, which resulted in the decrease in adsorption capacity.[7,31] However, this slight decrease demonstrated that other adsorption theories except electrostatic force worked and remained predominantly including the $\pi-\pi$ stacking effect provided by the graphite structure of Zn@PCNFs.

Due to the complexity in the composition of waste water, the influences of various cations and anions on adsorption capacity were investigated. As shown in Figure 2b,c, cations like Cu^{2+}, Ni^{2+}, Fe^{2+}, and Fe^{3+} generally could reduce the adsorption capacity, while anions like Cl^-, $Cr_2O_7^{2-}$, IO_3^-, and SO_4^{2-} could enhance it.

Temperature is another factor influencing MB adsorption. Different experimental temperatures were evaluated, and the result is shown in Figure 2d. Generally, the adsorption capacity was enhanced with the increase in temperature because a higher temperature endows MB with a faster movement speed.[32] In addition, a rapid adsorption behavior was presented at the first 30 min, and the curves became gradually flattened at the succeeding time. After about 400 min of adsorption, the equilibrium adsorption capacity was increased from 67.011 mg/g at 20 °C to 68.225 mg/g at 50 °C, which means that the temperature slightly influenced the adsorption capacity.

As shown in Figure 2e, the adsorption capacity of Zn@PCNFs with different added ZnO amounts was tested. Compared with the original PCNFs, the adsorption efficiency of Zn@PCNFs was obviously improved and reached maximum when ZnO was 3%. According to the results in Figure S3, the pore structure was changed after ZnO addition, which revealed that Zn@PCNFs obtained a higher specific surface area and wider pore size distribution. Therefore, the adsorption capacity was enhanced by Zn incorporation compared to ZnO particles and pure CNFs (Figure S7). In addition, the Zn source was also investigated. As shown in Figure S8, by controlling the same Zn element amount, ZnO-incorporated PCNFs presented a higher adsorption efficiency than $ZnCl_2$ and $Zn(Ac)_2$ (Figure S9a,b). In addition, different Zn-incorporated adsorbent structures of ZnO nanoparticles (Figure S9c), carbonized ZIF-8, and Zn@PCNFs were well prepared and evaluated, the result of which showed that Zn@PCNFs obtained a superior adsorption performance (Figure S10).

On the factor of the initial concentration of MB, a gradient concentration experiment was carried out and the result is shown in Figure 2f. The adsorption efficiency was decreased from 99.60% (Figure S11) to 20.91% when the MB initial concentration was increased from 25 to 800 mg/L. However, the adsorption efficiency was higher than 90% when the MB initial concentration was below 100 mg/L. A higher initial concentration provides a stronger driving force to transfer matter on the surface with a higher adsorbing quantity,[15] while the adsorption efficiency decreases at a dramatically high concentration.[33]

https://doi.org/10.1021/acsomega.1c05729
ACS Omega 2022, 7, 2198−2204

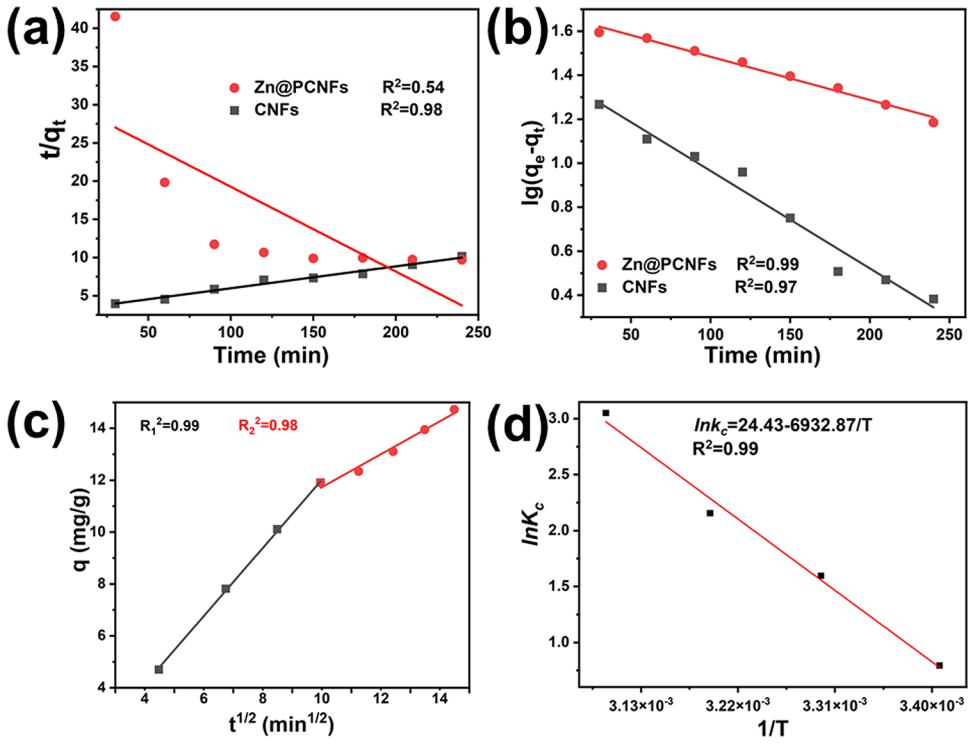

Figure 3. Kinetic parameters of (a) pseudo-first-order and (b) pseudo-second-order adsorption kinetic models for MB on Zn@PCNFs. (c) Intraparticle diffusion models of Zn@PCNFs. (d) Adsorption thermodynamics of Zn@PCNFs.

Table 1. Simulation Parameters of the Particle Diffusion Model of Zn@PCNFs

K_{ip1} (mg·g^{-1}·min$^{-0.5}$)	C_1	R_1^2	K_{ip2} (mg·g^{-1}·min$^{-0.5}$)	C_2	R_2^2
1.31 ± 0.02	−2.42 ± 0.20	0.999	0.64 ± 0.03	4.75 ± 0.75	0.977

Table 2. Langmuir and Freundlich Isotherm Parameters of Zn@PCNFs

Langmuir isotherm			Freundlich isotherm		
q_m (mg·g^{-1})	K_L	R_L^2	n	K_F	R_F^2
35.88 ± 1.53	3.78 ± 0.16	0.993	3.50 ± 0.54	22.52 ± 1.58	0.936

2.3. Adsorption Kinetics Analysis of Zn@PCNFs. Pseudo-first-order, pseudo-second-order, and intraparticle diffusion models were applied to analyze the results, which were calculated as eqs 1−3, respectively:

$$\ln(q_e - q_t) = \ln q_e - k_1 t \quad (1)$$

$$\frac{t}{q_t} = \frac{1}{k_2 q_e^2} + \frac{t}{q_e} \quad (2)$$

$$q_t = k_{ip} t^{0.5} + C \quad (3)$$

where q_e means the equilibrium adsorption capacity, q_t means the adsorption capacity at a certain time t, and k_1, k_2, and k_{ip} mean the constants of pseudo-first-order, pseudo-second-order, and diffusion rates. C means a constant of the interface thickness.

The fitting results are shown in Figure 3; the pseudo-first-order model (Figure 3a) was better in describing the adsorption process of Zn@PCNFs than the pseudo-second-order model (Figure 3b). Intraparticle diffusion models were fitted and are shown in Figure 3c, and two stages were found. For the first stage, the slope of the fitting line was larger, which means that the MB molecule could disperse to the Zn@PCNFs surface and be quickly adsorbed, which then further revealed a typical liquid film diffusion. For the second stage, the lower slope means that the adsorbing speed was lower than the first stage, which revealed an inner diffusion of the MB molecule in the pores of Zn@PCNFs.[34] The constant C obtained by the intercept at the y axis could be applied to reflect the mass transferring speed of the two stages. Obviously, a lower C_1 (Table 1) means a smaller interface thickness and MB diffusion resistance of the first stage[4,32] due to the concentration gradient driving force at the earlier period of adsorption. When more MB molecules were adsorbed, the driving force was weakened and the diffusion of MB should overcome a stronger resistance in the following adsorption period.

2.4. Adsorption Isotherm of Zn@PCNFs. Adsorption isotherm models of Langmuir and Freundlich are widely proven to analyze various adsorption equilibria of metal ions and dye molecules in evaluating adsorption capacity and forecasting the adsorption behavior based on the fitting results of different adsorption isotherm models.[35,36] The Langmuir and Freundlich models were calculated by eqs 4 and 5, respectively:

https://doi.org/10.1021/acsomega.1c05729
ACS Omega 2022, 7, 2198−2204

$$\frac{c_e}{q_e} = \frac{c_e}{q_m} + \frac{1}{K_L q_m} \quad (4)$$

$$\ln q_e = \frac{1}{n} \ln c_e + \ln K_F \quad (5)$$

where K_L and K_F mean the Langmuir and Freundlich adsorption equilibrium constants, respectively, q_m means the maximum adsorption capacity (mg/g), $1/n$ means the characteristic constant related to the adsorption strength.

As shown in Table 2, both isotherms had good fitting on the MB adsorption of Zn@PCNFs. The Langmuir model fits slightly better than Freundlich, indicating that MB is adsorbed as a monolayer. For the Freundlich model, n is calculated as 3.499, revealing that intermolecular force existed during the adsorption process on the uneven surface of Zn@PCNFs.[37]

2.5. Adsorption Thermodynamics of Zn@PCNFs. Gibbs equation was applied to analyze the influence of temperature on MB adsorption:

$$K_c = \frac{c_e}{q_e} \quad (6)$$

$$\ln K_c = -\frac{\Delta H}{RT} + \frac{\Delta s}{R} \quad (7)$$

$$\Delta G = -RT \ln K_c^{\circ} \quad (8)$$

where K_c means the thermodynamic equilibrium constant (L/mg), ΔG means the Gibbs free energy (kJ·mol^{-1}), ΔH means the adsorption enthalpy (kJ·mol^{-1}), ΔS means the adsorption entropy (kJ·mol^{-1}·K^{-1}), R means the thermodynamic constant (8.314 J·mol^{-1}·K^{-1}), T means the adsorption temperature (K), and Kc° means the standard equilibrium adsorption constant (L·mg^{-1}).

The adsorption process was carried out by exchanging between solvent and solute molecules on absorbance, which would cause heat exchanging and be influenced by temperature. As shown in Figure 3d and Table 3, ΔH and ΔS were positive values, and ΔG was calculated to be a negative value, revealing that MB adsorption on Zn@PCNFs had an endothermic behavior and was a spontaneous process at or above room temperature. In addition, the absolute value of ΔG was increased with increasing temperature, indicating that appropriate heat would accelerate the adsorption process.

Table 3. Equilibrium and Thermodynamic Parameters for the Sorption of MB by Zn@PCNFs

T (K)	ΔG (kJ·mol^{-1})	ΔH (kJ·mol^{-1})	ΔS (kJ·mol^{-1}·K^{-1})	R^2
323.15	−8.20 ± 0.35	57.64 ± 3.96	0.20 ± 0.01	0.991
313.15	−5.61 ± 0.20			
303.15	−4.02 ± 0.20			
293.15	−1.94 ± 0.08			

3. CONCLUSIONS

Zn-incorporated porous carbon nanofibers (Zn@PCNFs) were successfully prepared by electrospinning a blend solution of PAN/ZnO nanoparticles. Various characterizations proved the homogeneous distribution of the Zn element and the porous structure of the nanofibers. Zn@PCNFs showed good adsorption capacity under various conditions including the pH value, temperature, and ion category. The pseudo-second-order and Freundlich models were better in describing the MB adsorption behavior, which is influenced by several factors. The prepared Zn@PCNFs provides considerable adsorption capacity on MB and great potential in organic dye solution treatment.

4. EXPERIMENTS

4.1. Materials and Instruments. Polyacrylonitrile (PAN, Mw = 1.5 × 10^5) and ZnO nanoparticles (purity of ≥99.9% metals basis, 30 ± 10 nm) were purchased from Sigma-Aldrich (Shanghai) Trading Co., Ltd. (Shanghai, China). Dimethylformamide (DMF, AR), methylene blue (MB, ID), $ZnCl_2$ (AR), $Zn(Ac)_2$ (purity of ≥99%), and 2-methylimidazole (purity of ≥98%) were purchased from Sinopharm Chemical Reagent Co., Ltd. (Shanghai, China).

4.2. Fabrication and Characterization of Zn-Incorporated Porous Carbon Nanofibers (Zn@PCNFs). The nanofibers were fabricated by an electrospinning technique as described in our previous work.[38] Briefly, PAN was dissolved in DMF to prepare 10 wt % solution and then various ratios of ZnO nanoparticles (1, 3, and 6 wt %) were added, stirred, and sonicated to form a homogeneous blend solution. As a comparison, different Zn sources were chosen to prepare the samples and reveal the property differences. $ZnCl_2$ was directly dissolved in DMF, and $Zn(Ac)_2$ was first used to synthesize ZIF-8 nanoparticles with 2-methylimidazole as reported from refs 39, 40 and added to PAN solution. The Zn quantity of $ZnCl_2$ and ZIF-8 was controlled the same as that of ZnO. In addition, carbon nanofibers (CNFs) prepared by pure PAN were used as a negative control group.

The electrospinning process was carried out under a voltage of 18 kV, an extrusion rate of 15 μL/min, and a receiving distance of 15 cm to prepare nanofiber mats followed by pre-oxidation under 250 °C in the air for 2 h and carbonization under 800 °C in a N_2 atmosphere for 2 h to prepare Zn@PCNFs.

The morphology of Zn@PCNFs was observed by SEM (Gemini SEM 300, Zeiss, Germany) and TEM (Talos F200X, ThermoFisher Scientific, USA). The TGA results were recorded through a thermogravimetric analyzer (TG 209 F1, Netzsch, Germany). The crystal structure was recorded by XRD (D2 Phaser, Bruker, Germany). The elemental composition was measured by XPS (Escalab 250Xi, ThermoFisher Scientific, USA). The BET surface areas, pore volumes, and pore size distributions were measured from nitrogen physisorption data at 77 K obtained with an ASAP 2020 analyzer (Micromeritics Instrument Corp., USA)

4.3. Adsorption Test of Zn@PCNFs. A series of concentrations of MB solution were prepared with different pH values adjusted with NaOH and HCl. Certain amounts of Zn@PCNFs were dispersed in MB solution and continuously shaken under room temperature. The solution was taken out at a preset time point and centrifuged, the supernatant of which was measured by UV−Vis spectrophotometry to determine the MB concentration. The equilibrium adsorption capacity (q_e) was calculated using eq 8:

$$q_e = \frac{(C_0 - C_e)V}{m} \quad (9)$$

where C_0 and C_e mean the MB concentrations (mg/L) before and after Zn@PCNFs adsorption, respectively, V means the

https://doi.org/10.1021/acsomega.1c05729
ACS Omega 2022, 7, 2198−2204

volume of the solution (L), and m means the weight of Zn@PCNFs (g).

To evaluate the influence of the ion category on MB adsorption capacity, various ions with different concentrations (0.05 and 0.2 mmol/L) were introduced in MB solution. Likewise, temperature was also investigated by setting the solution in a shaker with different temperatures.

■ ASSOCIATED CONTENT

Supporting Information

The Supporting Information is available free of charge at https://pubs.acs.org/doi/10.1021/acsomega.1c05729.

Additional characterizations of the size, morphology, crystal structure, PZC, and optical properties of the products and the samples obtained (PDF)

■ AUTHOR INFORMATION

Corresponding Authors

Yi Luo − *School of Textile and Clothing and Key Laboratory of Neuroregeneration of Jiangsu and Ministry of Education, Co-innovation Center of Neuroregeneration, Nantong University, Nantong 226001, China*; Email: lynantong@hotmail.com

Wei Zhang − *School of Textile and Clothing and Key Laboratory of Neuroregeneration of Jiangsu and Ministry of Education, Co-innovation Center of Neuroregeneration, Nantong University, Nantong 226001, China*; Email: zhangwei@ntu.edu.cn

Jiamu Dai − *School of Textile and Clothing and Key Laboratory of Neuroregeneration of Jiangsu and Ministry of Education, Co-innovation Center of Neuroregeneration, Nantong University, Nantong 226001, China*; orcid.org/0000-0002-0627-4999; Email: jmdai@ntu.edu.cn

Authors

Du Nie − *School of Textile and Clothing and Key Laboratory of Neuroregeneration of Jiangsu and Ministry of Education, Co-innovation Center of Neuroregeneration, Nantong University, Nantong 226001, China*

Ping Wang − *Department of Imaging, Nantong First People's Hospital, Nantong 226001, China*

Chuanfeng Zang − *School of Textile and Clothing and Key Laboratory of Neuroregeneration of Jiangsu and Ministry of Education, Co-innovation Center of Neuroregeneration, Nantong University, Nantong 226001, China*

Guangyu Zhang − *School of Textile and Clothing and Key Laboratory of Neuroregeneration of Jiangsu and Ministry of Education, Co-innovation Center of Neuroregeneration, Nantong University, Nantong 226001, China*; orcid.org/0000-0002-1364-3350

Suying Li − *School of Textile and Clothing and Key Laboratory of Neuroregeneration of Jiangsu and Ministry of Education, Co-innovation Center of Neuroregeneration, Nantong University, Nantong 226001, China*

Rong Liu − *School of Textile and Clothing and Key Laboratory of Neuroregeneration of Jiangsu and Ministry of Education, Co-innovation Center of Neuroregeneration, Nantong University, Nantong 226001, China*

Yu Zhang − *School of Textile and Clothing and Key Laboratory of Neuroregeneration of Jiangsu and Ministry of Education, Co-innovation Center of Neuroregeneration, Nantong University, Nantong 226001, China*

Guang Li − *State Key Laboratory for Modification of Chemical Fibers and Polymer Materials, College of Materials Science and Engineering, Donghua University, Shanghai 201620, China*; orcid.org/0000-0002-7456-826X

Complete contact information is available at: https://pubs.acs.org/10.1021/acsomega.1c05729

Notes

The authors declare no competing financial interest.

#D.N. and P.W. contributed equally to this study.

■ ACKNOWLEDGMENTS

This study was financially supported by the National Key Research and Development Program of China (no. 2016YFB0303101), National Natural Science Foundation of China (nos. 51803094 and 81702723), Jiangsu University "Qinglan Project", and Science and Technology Project of Nantong City (no. MS12021006).

■ REFERENCES

(1) Zhang, Y.-R.; Shen, S.-L.; Wang, S.-Q.; Huang, J.; Su, P.; Wang, Q.-R.; Zhao, B.-X. A dual function magnetic nanomaterial modified with lysine for removal of organic dyes from water solution. *Chem. Eng. J.* **2014**, *239*, 250−256.

(2) Vadivelan, V.; Kumar, K. V. Equilibrium, kinetics, mechanism, and process design for the sorption of methylene blue onto rice husk. *J. Colloid Interface Sci.* **2005**, *286*, 90−100.

(3) Asouhidou, D. D.; Triantafyllidis, K. S.; Lazaridis, N. K.; Matis, K. A.; Kim, S.-S.; Pinnavaia, T. J. Sorption of reactive dyes from aqueous solutions by ordered hexagonal and disordered mesoporous carbons. *Microporous Mesoporous Mater.* **2009**, *117*, 257−267.

(4) Cherifi, H.; Fatiha, B.; Salah, H. Kinetic studies on the adsorption of methylene blue onto vegetal fiber activated carbons. *Appl. Surf. Sci.* **2013**, *282*, 52−59.

(5) Zhou, Y.; Jin, Q.; Hu, X.; Zhang, Q.; Ma, T. Heavy metal ions and organic dyes removal from water by cellulose modified with maleic anhydride. *J. Mater. Sci.* **2012**, *47*, 5019−5029.

(6) Zhou, Y.; Zhang, M.; Hu, X.; Wang, X.; Niu, J.; Ma, T. Adsorption of Cationic Dyes on a Cellulose-Based Multicarboxyl Adsorbent. *J. Chem. Eng. Data* **2013**, *58*, 413−421.

(7) Sun, Y.; Wu, Z. Y.; Wang, X.; Ding, C.; Cheng, W.; Yu, S. H.; Wang, X. Macroscopic and Microscopic Investigation of U(VI) and Eu(III) Adsorption on Carbonaceous Nanofibers. *Environ. Sci. Technol.* **2016**, *50*, 4459−4467.

(8) Willner, M. R.; Vikesland, P. J. Nanomaterial enabled sensors for environmental contaminants. *J. Nanobiotechnol.* **2018**, *16*, 95.

(9) Goodman, S. M.; Bura, R.; Dichiara, A. B. Facile Impregnation of Graphene into Porous Wood Filters for the Dynamic Removal and Recovery of Dyes from Aqueous Solutions. *ACS Appl. Nano Mater.* **2018**, *1*, 5682−5690.

(10) Li, Y.; Wang, H.; Xie, L.; Liang, Y.; Hong, G.; Dai, H. MoS2 nanoparticles grown on graphene: an advanced catalyst for the hydrogen evolution reaction. *J. Am. Chem. Soc.* **2011**, *133*, 7296−7299.

(11) An, G.-H.; Ahn, H.-J.; Hong, W.-K. Electrochemical properties for high surface area and improved electrical conductivity of platinum-embedded porous carbon nanofibers. *J. Power Sources* **2015**, *274*, 536−541.

(12) Perreault, F.; Fonseca de Faria, A.; Elimelech, M. Environmental applications of graphene-based nanomaterials. *Chem. Soc. Rev.* **2015**, *44*, 5861−5896.

(13) Ersan, G.; Kaya, Y.; Apul, O. G.; Karanfil, T. Adsorption of organic contaminants by graphene nanosheets, carbon nanotubes and granular activated carbons under natural organic matter preloading conditions. *Sci. Total Environ.* **2016**, *565*, 811−817.

(14) Ersan, G.; Apul, O. G.; Perreault, F.; Karanfil, T. Adsorption of organic contaminants by graphene nanosheets: A review. *Water Res.* **2017**, *126*, 385−398.
(15) Kang, C.; Zhu, L.; Wang, Y.; Wang, Y.; Xiao, K.; Tian, T. Adsorption of Basic Dyes Using Walnut Shell-based Biochar Produced by Hydrothermal Carbonization. *Chem. Res. Chin. Univ.* **2018**, *34*, 622−627.
(16) Wang, J.; Kaskel, S. KOH activation of carbon-based materials for energy storage. *J. Mater. Chem.* **2012**, *22*, 23710.
(17) Karimnezhad, L.; Haghighi, M.; Fatehifar, E. Adsorption of benzene and toluene from waste gas using activated carbon activated by ZnCl2. *Front. Environ. Sci. Eng.* **2014**, *8*, 835−844.
(18) Ahmad, M.; Lee, S. S.; Dou, X.; Mohan, D.; Sung, J. K.; Yang, J. E.; Ok, Y. S. Effects of pyrolysis temperature on soybean stover- and peanut shell-derived biochar properties and TCE adsorption in water. *Bioresour. Technol.* **2012**, *118*, 536−544.
(19) Ahmad, M.; Rajapaksha, A. U.; Lim, J. E.; Zhang, M.; Bolan, N.; Mohan, D.; Vithanage, M.; Lee, S. S.; Ok, Y. S. Biochar as a sorbent for contaminant management in soil and water: a review. *Chemosphere* **2014**, *99*, 19−33.
(20) Suhas; Gupta, V. K.; Carrott, P. J. M.; Singh, R.; Chaudhary, M.; Kushwaha, S. Cellulose: A review as natural, modified and activated carbon adsorbent. *Bioresour. Technol.* **2016**, *216*, 1066−1076.
(21) Lillo-Ródenas, M. A.; Cazorla-Amorós, D.; Linares-Solano, A. Benzene and toluene adsorption at low concentration on activated carbon fibres. *Adsorption* **2011**, *17*, 473−481.
(22) An, G. H.; Lee, D. Y.; Ahn, H. J. Tunneled Mesoporous Carbon Nanofibers with Embedded ZnO Nanoparticles for Ultrafast Lithium Storage. *ACS Appl. Mater. Interfaces* **2017**, *9*, 12478−12485.
(23) Nain, R.; Singh, D.; Jassal, M.; Agrawal, A. K. Zinc oxide nanorod assisted rapid single-step process for the conversion of electrospun poly(acrylonitrile) nanofibers to carbon nanofibers with a high graphitic content. *Nanoscale* **2016**, *8*, 4360−4372.
(24) Mohamed, M. M.; Ghanem, M. A.; Khairy, M.; Naguib, E.; Alotaibi, N. H. Zinc oxide incorporated carbon nanotubes or graphene oxide nanohybrids for enhanced sonophotocatalytic degradation of methylene blue dye. *Appl. Surf. Sci.* **2019**, *487*, 539−549.
(25) An, G. H.; Kim, S. J.; Park, K. W.; Ahn, H. J. Composites of Carbon Nanofibers and Nanophase Pt-SnO2 for Lithium-Ion Batteries. *ECS Solid State Lett.* **2014**, *3*, M21−M23.
(26) Zhang, W.; Dai, J.; Zhang, G.; Zhang, Y.; Li, S.; Nie, D. Photothermal/pH Dual-Responsive Drug Delivery System of Amino-Terminated HBP-Modified rGO and the Chemo-Photothermal Therapy on Tumor Cells. *Nanoscale Res. Lett.* **2018**, *13*, 379.
(27) Tan, H.; Tang, J.; Kim, J.; Kaneti, Y. V.; Kang, Y.-M.; Sugahara, Y.; Yamauchi, Y. Rational design and construction of nanoporous iron- and nitrogen-doped carbon electrocatalysts for oxygen reduction reaction. *J. Mater. Chem. A* **2019**, *7*, 1380−1393.
(28) Miao, J.; Geng, W.; Alvarez, P. J. J.; Long, M. 2D N-Doped Porous Carbon Derived from Polydopamine-Coated Graphitic Carbon Nitride for Efficient Nonradical Activation of Peroxymonosulfate. *Environ. Sci. Technol.* **2020**, *54*, 8473−8481.
(29) Peng, W.; Yang, X.; Mao, L.; Jin, J.; Yang, S.; Zhang, J.; Li, G. ZIF-67-derived Co nanoparticles anchored in N doped hollow carbon nanofibers as bifunctional oxygen electrocatalysts. *Chem. Eng. J.* **2021**, *407*, 127157.
(30) Hu, Y.; Guo, T.; Ye, X.; Li, Q.; Guo, M.; Liu, H.; Wu, Z. Dye adsorption by resins: Effect of ionic strength on hydrophobic and electrostatic interactions. *Chem. Eng. J.* **2013**, *228*, 392−397.
(31) Fan, S.; Wang, Y.; Wang, Z.; Tang, J.; Tang, J.; Li, X. Removal of methylene blue from aqueous solution by sewage sludge-derived biochar: Adsorption kinetics, equilibrium, thermodynamics and mechanism. *J. Environ. Chem. Eng.* **2017**, *5*, 601−611.
(32) Ghorai, S.; Sarkar, A.; Raoufi, M.; Panda, A. B.; Schonherr, H.; Pal, S. Enhanced removal of methylene blue and methyl violet dyes from aqueous solution using a nanocomposite of hydrolyzed polyacrylamide grafted xanthan gum and incorporated nanosilica. *ACS Appl. Mater. Interfaces* **2014**, *6*, 4766−4777.
(33) Ma, J.; Yu, F.; Zhou, L.; Jin, L.; Yang, M.; Luan, J.; Tang, Y.; Fan, H.; Yuan, Z.; Chen, J. Enhanced adsorptive removal of methyl orange and methylene blue from aqueous solution by alkali-activated multiwalled carbon nanotubes. *ACS Appl. Mater. Interfaces* **2012**, *4*, 5749−5760.
(34) Zhu, Y.; Yi, B.; Yuan, Q.; Wu, Y.; Wang, M.; Yan, S. Removal of methylene blue from aqueous solution by cattle manure-derived low temperature biochar. *RSC Adv.* **2018**, *8*, 19917−19929.
(35) Chang, M. Y.; Juang, R. S. Adsorption of tannic acid, humic acid, and dyes from water using the composite of chitosan and activated clay. *J. Colloid Interface Sci.* **2004**, *278*, 18−25.
(36) da Silva Filho, E. C.; da Silva, L. S.; Lima, L. C. B.; de S Santos Júnior, L.; de MC Santos, M. R.; de Matos, J. M. E.; Airoldi, C. Thermodynamic Data of 6-(4′-Aminobutylamino)-6-deoxycellulose Sorbent for Cation Removal from Aqueous Solutions. *Sep. Sci. Technol.* **2011**, *46*, 2566−2574.
(37) Meghea, A.; Rehner, H. H.; Peleanu, I.; Mihalache, R. Test-fitting on adsorption isotherms of organic pollutants from waste waters on activated carbon. *J. Radioanal. Nucl. Chem.* **1998**, *229*, 105−110.
(38) Dai, J.; Luo, Y.; Nie, D.; Jin, J.; Yang, S.; Li, G.; Yang, Y.; Zhang, W. pH/photothermal dual-responsive drug delivery and synergistic chemo-photothermal therapy by novel porous carbon nanofibers. *Chem. Eng. J.* **2020**, *397*, 125402.
(39) Luzuriaga, M. A.; Benjamin, C. E.; Gaertner, M. W.; Lee, H.; Herbert, F. C.; Mallick, S.; Gassensmith, J. J. ZIF-8 Degrades in Cell Media, Serum, and Some-But Not All-Common Laboratory Buffers. *Supramol. Chem.* **2019**, *31*, 485−490.
(40) Zhang, H.; Wang, C.; Zhang, W.; Zhang, M.; Qi, J.; Qian, J.; Sun, X.; Yuliarto, B.; Na, J.; Park, T.; Gomaa, H. G. A.; Kaneti, Y. V.; Yi, J. W.; Yamauchi, Y.; Li, J. Nitrogen, phosphorus co-doped eave-like hierarchical porous carbon for efficient capacitive deionization. *J. Mater. Chem. A* **2021**, *9*, 12807−12817.

https://doi.org/10.1021/acsomega.1c05729
ACS Omega 2022, 7, 2198−2204